1-1-2005

Elevated Temperature Deformation Behavior of Nanostructured Al-Ni-Gd-Fe Alloys

X. L. Shi

Rajiv S. Mishra
Missouri University of Science and Technology

T. J. Watson

Available online at www.sciencedirect.com
SCIENCE DIRECT®
Scripta Materialia 52 (2005) 887–891
Scripta MATERIALIA
www.actamat-journals.com

Elevated temperature deformation behavior of nanostructured Al–Ni–Gd–Fe alloys

X.L. Shi [a], R.S. Mishra [a,*], T.J. Watson [b]

[a] Department of Materials Science and Engineering, University of Missouri, 218 McNutt Hall, Rolla, MO 65409, United States
[b] Materials and Processes Engineering, Pratt and Whitney, East Hartford, CT 06108, United States

Received 29 November 2004; received in revised form 22 December 2004; accepted 4 January 2005
Available online 22 January 2005

Abstract

The elevated temperature deformation behavior of nanostructured $Al_{89}Ni_3Gd_7Fe_1$ alloy was characterized. Tensile strength was 760 MPa at 373 K. Ductility of the alloy increases with increasing strain rate at 573 K. At high temperatures (623–673 K), the operative deformation mechanism is dislocation-climb controlled.

Keywords: Aluminum alloys; High temperature deformation; Ultrafine grained microstructure; Nanostructured alloys

1. Introduction

The promise of non-equilibrium processing has resulted in a major thrust for the development of high performance Al-based alloys with enhanced strength, stiffness and thermal stability at elevated temperatures. For high temperature applications, the focus is on producing alloys with a high volume fraction of dispersoids and very fine microstructures [1,2]. Contributions to strength enhancement of the soft metal matrix arise because of non-shearable barriers to the movement of dislocations. In particular, crystallization of amorphous alloys provides opportunities to produce bulk nanostructured materials with a high volume fraction of intermetallic particles. Phase transformation from the amorphous state has some unique features [3]: (a) homogenous nucleation, (b) high nucleation frequency, (c) low growth rate, and (d) nanoscale interparticle spacing. All of these are beneficial for developing high-strength dispersion-strengthened alloys. It also enables great flexibility in the design of materials with chosen volume fractions, types, and sizes of dispersoids and of alloying additions. Amorphous aluminum alloys can be obtained in Al–TM–RE (TM = transition metals, RE = rare earth elements) systems [4,5]. Shiflet and coworkers [6] have reported that Al–Ni–Fe–Gd alloys have unique metallic glass formability. So far, ambient temperature mechanical properties of such alloys have been reported and very little work has been done on determining the elevated temperature tensile behavior of bulk nanocrystalline alloys [7,8].

The purpose of this paper is to report the elevated temperature deformation behavior of an as-extruded dispersion-strengthened $Al_{89}Ni_3Gd_7Fe_1$ (at.%) alloy at various temperatures and strain rates.

2. Experimental procedure

Atomized $Al_{89}Ni_3Gd_7Fe_1$ powders were extruded into 15.9 mm diameter rods. The starting billet temperature was in the range from 733 to 761 K, with 10 min

* Corresponding author. Tel.: +1 573 341 6361; fax: +1 573 341 6934.
E-mail address: rsmishra@umr.edu (R.S. Mishra).

1359-6462/$ - see front matter
doi:10.1016/j.scriptamat.2005.01.002

of heat-up time and 4 min soaking time. An extrusion ratio of 20:1 was used for all rods. Mini-tensile specimens with rectangular cross-section (gage length 1.3 mm and gage width 1.0 mm) were electro-discharge machined from as-extruded rods in the longitudinal direction. The tensile specimens were polished to the final thickness of ~0.5 mm and 1 μm finish. Tension tests were performed on a custom-built, computer-controlled mini-tensile tester in the temperature range of 373–673 K and initial strain rate range of 5×10^{-5} to 1×10^{-2} s^{-1}.

Microstructure of the extruded rod was examined using a Philips EM430 transmission electron microscope (TEM) at 300 kV. Thin foils were prepared from as received alloys by double jet electropolishing using a Struers-Tenupol 2 device operating at ~12 V. The electrolyte was 20 vol% HNO_3 and 80 vol% methanol cooled to 243 K. The effect of temperature on the tensile behavior of this alloy was analyzed based on the fractographic examinations, which were conducted using a Hitachi S4700 scanning electron microscope (SEM).

3. Results and discussion

3.1. Microstructure

Fig. 1 shows the microstructure of an as-extruded $Al_{89}Ni_3Gd_7Fe_1$ alloy. Hot extrusion of the amorphous powders results in the formation of ultra-fine structure consisting of ~35 vol% of nanostructured intermetallic particles, embedded in the matrix. The matrix was almost pure α-Al due to very low solid solubility of Gd, Ni, and Fe in Al. The average grain size was ~200 nm. Rod-like particles (length ~160 nm and width ~30 nm) and equiaxed particles (~80 nm) were mostly located along the grain boundaries. Dislocation density was very low in the interior of the grains.

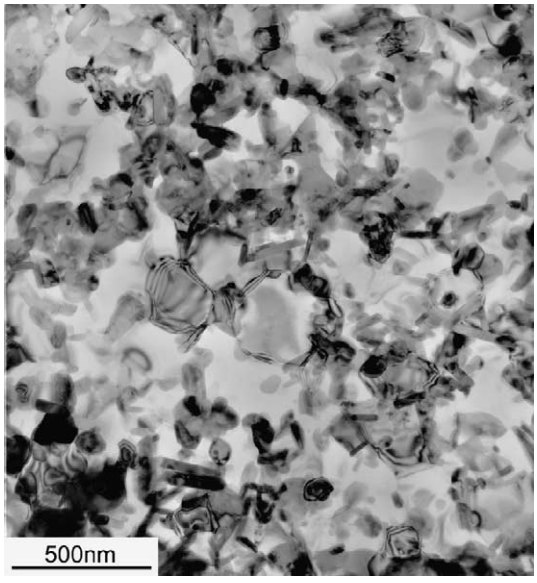

Fig. 1. Bright-field TEM micrograph of as-extruded $Al_{89}Ni_3Gd_7Fe_1$ alloy.

3.2. Elevated temperature deformation behavior

The variation of tensile behavior with temperature at an initial of strain rate 1×10^{-3} s^{-1} is shown in Fig. 2, where UTS is the ultimate tensile strength, YS the yield strength, and ε_f the failure strain (true plastic strain from the stress–strain curves). It can be noted that the tensile strength of this alloy is 760 MPa at 373 K, which is higher than that of traditional elevated temperature alloys. For example, the tensile strength of extruded 2618 aluminum alloy is 405 MPa at 373 K [9]. Strength of $Al_{89}Ni_3Gd_7Fe_1$ alloy decreases gradually with increasing temperature and the ductility increases sharply above 623 K and reaches 24% elongation at 673 K (at room temperature the material failed in a brittle manner). Retention of strengthening at elevated temperatures can be attributed to the high volume fraction of nanostructured dispersoids. Also the nanostructure reduces the size of nucleating flaws and increases the resistance to crack propagation, leading to higher fracture strength [10]. Very fine second phase particles situated at the grain boundary in this alloy can be effective in the prevention of grain boundary migration, limiting grain growth due to the Zener pinning. Because of the few intragranular particles, Orowan dislocation looping cannot be considered as the primary strengthening mechanism. However, for such nanostructured materials, the theoretical framework for dislocation–particle interaction has not been developed. For example, the strengthening due to the interaction of dislocations with grain boundary particles has not been quantified.

True stress–strain curves for various initial strain rates at 573 K are shown in Fig. 3. At this temperature, the yield stress and failure strain increases with increasing strain rate. Similar behavior was also observed in

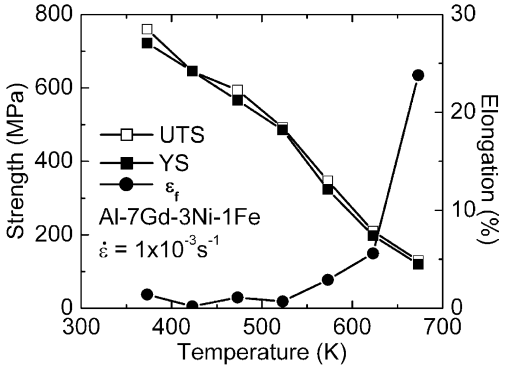

Fig. 2. Variation of strength and ductility with temperature for $Al_{89}Ni_3Gd_7Fe_1$ alloy.

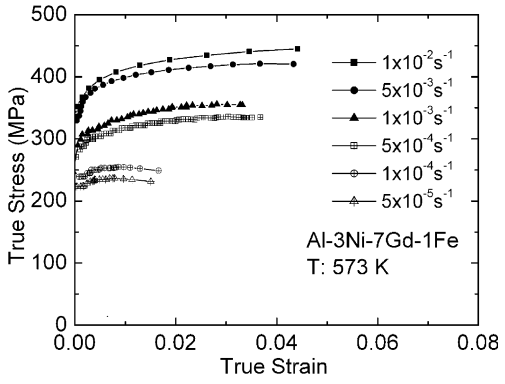

Fig. 3. Stress–strain behavior of $Al_{89}Ni_3Gd_7Fe_1$ alloy at 573 K for various initial strain rates.

rapid solidification/powder metallurgy (RS/PM) aluminum alloys [11]. This is quite different from that of ingot metallurgy processed aluminum alloys with coarser microstructures. It has previously been shown that in materials with particles present along grain boundaries, plastic flow is produced by dislocation nucleation from the grain boundaries and from constituent particles pinning the grain boundaries [12]. The interaction between dislocations and particles results in more damage of the grain boundaries at lower strain rates. For $Al_{89}Ni_3Gd_7Fe_1$ alloy, uniform elongation decreases from 4% to 1% when initial strain rate decreases from $1\times10^{-2}\,s^{-1}$ to $5\times10^{-5}\,s^{-1}$ at 573 K, which implies an early start of the failure mechanisms with decreasing strain rate. Cavity nucleation and strain localization due to insufficient work hardening are possible explanations for the observed behavior. At lower strain rates, flow stress increases initially and then decreases with increasing strain. It is possible that the rate of dynamic recovery or evolution of damage leads to flow softening.

The variation of flow stress with strain rate at high temperatures is shown in Fig. 4. The apparent stress exponent decreases with increasing temperatures. The observed stress exponents are higher than 5. The presence of particles at the grain boundaries makes elevated

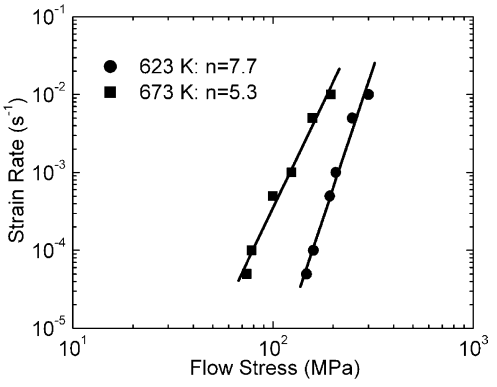

Fig. 4. Variation of strain rate with flow stress at high temperatures.

temperature deformation more difficult. However the values are not like other dispersion-strengthened Al-based alloys, in which very high apparent stress exponents were observed [1]. A possible explanation is that most of particles are present along the grain boundaries. In this case, it is assumed that the strain rate is controlled by the breakaway of grain boundary dislocations from the particles, and the stress exponent could be reduced by ~1/4–1/9 compared to the microstructure containing particles within the grains [13].

The deformation behavior of dispersion-strengthened materials at high temperatures can be represented by the constitutive equation which incorporates threshold stress as given by [14,15]

$$\dot{\varepsilon} = A\left(\frac{GbD_L}{kT}\right)\left(\frac{\sigma-\sigma_0}{G}\right)^n \quad (1)$$

where $\dot{\varepsilon}$ is the strain rate, D_L the lattice self-diffusivity, G the shear modulus, b the Burgers vector, k the Boltzmann's constant, T the absolute temperature, σ the applied stress, σ_0 the threshold stress, A the dimensionless constant, n the true stress exponent. The threshold stress concept is often introduced to rationalize the high stress exponents in dispersion-strengthened alloys [16]. Lagneborg and Bergman [17] introduced the widely used method to determine experimental threshold stress by plotting $\dot{\varepsilon}^{1/n}$ versus σ with $n = 5$ for pure aluminum, and extrapolating the linear fitted line to zero $\dot{\varepsilon}$. Experimental threshold stress values at high temperatures are listed in Table 1. It can be noted that it decreases with temperature. In the climb threshold models, the origin of the threshold stress is considered as the increase in dislocation line length during the climb bypass [18–21]. The threshold stress models proposed by Arzt and coworkers [22,23] and Mishra et al. [24] suggest that the origin of threshold stress is due to the attractive dislocation–particle interaction. These models for threshold stress for dislocation creep are based on interaction of lattice dislocations with particles within the grain. However, as noted earlier, in the present alloy particles are mostly on the grain boundaries. Existing threshold models cannot predict threshold stress for this kind of nanostructured alloy.

The normalized strain rate, $\dot{\varepsilon}kT/D_LGb$, is plotted against the normalized effective stress $(\sigma-\sigma_0)/G$, on double logarithmic scales in Fig. 5. For the data analysis, the values of the lattice self-diffusivity D_L [M^2/s] = $1.71\times10^{-4}\exp(-142/RT)$ [25], and G [MPa] = 3.0×10^4 − ce:hsp sp="0.25"/>16T [26], where R is the universal gas constant, were used. After considering

Table 1
Experimental threshold stress values at high temperatures

Temperature (K)	623	673
Threshold stress (MPa)	69	6

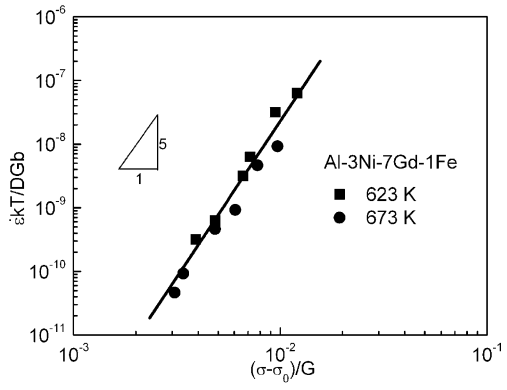

Fig. 5. Temperature and diffusivity compensated strain rate versus normalized effective stress.

threshold stress, the experimental results at 623 and 673 K can be fitted well into the straight line with slope 5, which indicates the dislocation-climb controlled deformation. The value of dimensionless constant A in Eq. (1) is 243.

SEM fractographs of tested samples at 573, 623 and 673 K and initial strain rate of $1 \times 10^{-3}\ s^{-1}$ are shown in Fig. 6. The present results show transition in fracture surface morphology from transgranular to intergranular in the temperature range 573–673 K. At 573 K, shallow ductile dimples with different sizes are present (Fig. 6(a) and (b)). It can be noted that the dimple size is close to the grain size. In very small dimples, dispersoids responsible for void initiation can be observed. At 623 K, the dimples are deeper and larger than those at 573 K (Fig. 6(c) and (d)). A number of particles are visible within the dimples and along the edge of the dimples. The characteristic dimple size is around 1.2 μm. At 673 K, dimple size ranges from 1 to 4 μm (Fig. 6(e) and (f)). There are some less well-developed dimples with a discontinuous dimple perimeter. However, individual grains can be identified at the bottom of the dimples at higher magnification as shown in Fig. 7. It appears that intergranular fracture starts contributing at this temperature. This fracture mode has been observed in aluminum alloys at low stresses and high temperatures. Growth of grain boundary voids by coupled diffusion and power-low creep leads to intergranular fracture. It covers a large part of the fracture maps proposed by Ashby et al. [27].

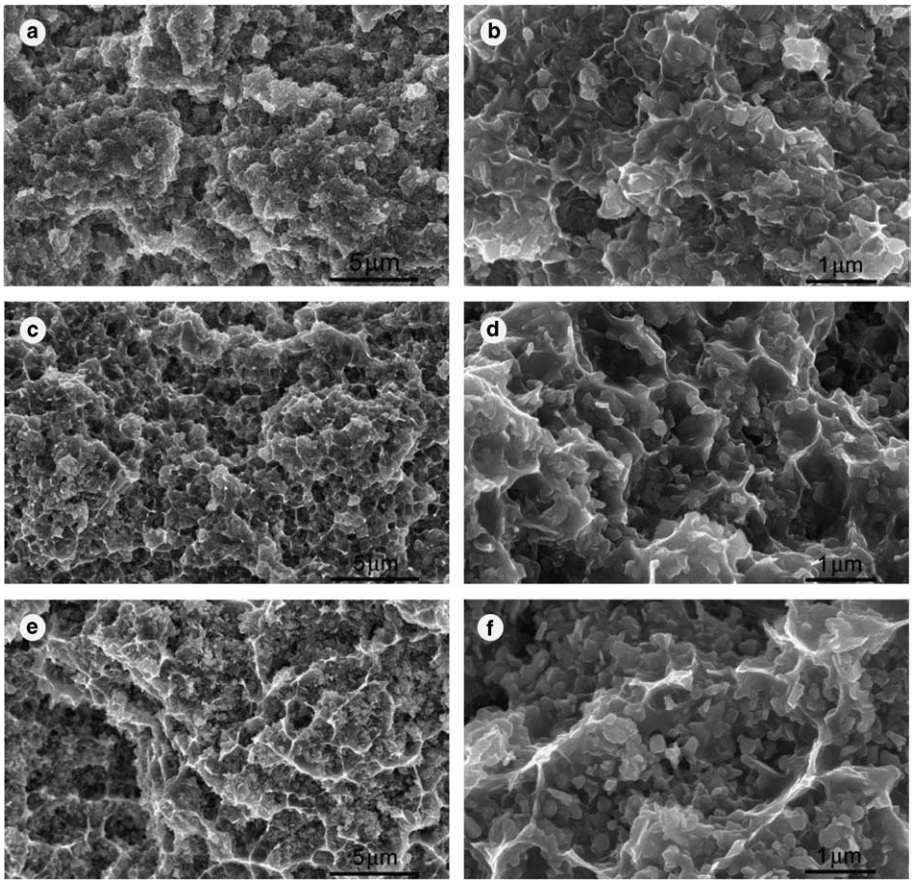

Fig. 6. SEM fracture surface of tested at: (a, b) 573 K; (c, d) 623 K; and (e, f) 673 K.

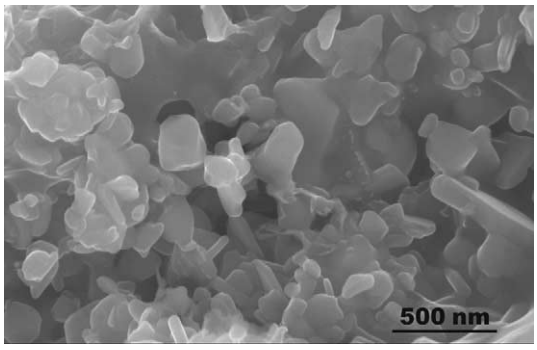

Fig. 7. High magnification SEM fracture surface of deformed sample at 673 K.

4. Conclusions

1. A high volume fraction of nanostructured intermetallic dispersoids can be obtained by the use of the amorphous precursor, which enables the $Al_{89}Ni_3Gd_7Fe_1$ alloy to exhibit high elevated temperature strength.
2. At 573 K, the ductility increases with the increasing stain rate.
3. The apparent stress exponent was higher than 5, indicating dislocation-climb mechanism with temperature-dependent threshold stress.
4. The fracture surface appearance varies with temperature. The fracture features change from transgranular to intergranular in the temperature range 573–673 K.

Acknowledgment

The authors gratefully acknowledge the financial support of DARPA through contract number F336115-01-2-5217.

References

[1] Arzt E, Rösler J. In: Kim YW, Griffth WM, editors. Dispersion strengthened aluminum alloys. Warrendale, PA: TMS; 1988. p. 31.
[2] Lavernia EJ, Ayers JD, Srivatsan TS. Int Mater Rev 1992;37:1.
[3] Inoue A, Kimura H. J Light Met 2001;1:31.
[4] Inoue A, Othera K, Tsai AP, Masumoto T. Jpn J Appl Phys 1988;27:L280.
[5] He Y, Poon SJ, Shiflet GJ. Science 1988;241:1640.
[6] He Y, Dougherty GM, Shiflet GJ, Poon SJ. Acta Metall Mater 1993;41:337.
[7] Ko BC, Wesseling P, Vatamanu OL, Shiflet GJ, Lewandowski JJ. Intermetallics 2002;10:1099.
[8] Dougherty GM, Shiflet GJ, Poon SJ. Acta Metall Mater 1994;42:2275.
[9] Kaufman JG, editor. Properties of aluminum alloys: tensile, creep, and fatigue data at high and low temperatures. Material Park, OH: ASM; 1999. p. 92.
[10] Koch CC, Morris DG, Lu K, Inoue A. MRS Bull 1999;24:54.
[11] Skinner DJ, Zedalis MS, Gilman P. Mater Sci Eng A 1989;119:81.
[12] Lloyd DJ, Morris LR. Acta Metall 1977;25:857.
[13] Rösler J, Joos R, Arzt E. Metall Trans A 1992;23:1521.
[14] Park KT, Lavernia EJ, Mohamed FA. Acta Metall Mater 1990;38:2149.
[15] Park KT, Lavernia EJ, Mohamed FA. Acta Metall Mater 1994;42:667.
[16] Gittus JH. Proc R Soc A 1975;342:279.
[17] Lagneborg R, Bergman B. Met Sci 1976;10:20.
[18] Brown LM, Ham RK. In: Kelly A, Nicholson RB, editors. Strengthening methods in crystals. New York: Halstead Press Division; 1971. p. 9.
[19] Shewfelt RSW, Brown LM. Philos Mag 1974;30:1135.
[20] Lagneborg R. Scr Metall 1973;7:605.
[21] McLean M. Acta Metall 1985;33:545.
[22] Arzt E, Wilkinson DS. Acta Metall Mater 1986;34:1893.
[23] Rösler J, Arzt E. Acta Metall Mater 1990;38:671.
[24] Mishra RS, Nandy TK, Greenwood GW. Philos Mag A 1994;69:1097.
[25] Frost HJ, Ashby MF. Deformation-mechanism maps: the plasticity and creep of metals and ceramics. Oxford: Pergamon Press; 1982. p. 21.
[26] Lundy TS, Murdock JF. J Appl Phys 1962;33:1671.
[27] Ashby MF, Gandhi C, Taplin DMR. Acta Metall 1977;27:699.